Variations of the growth of harmonic reflections in fiber Bragg gratings fabricated using phase masks

Claire M. Rollinson,[1] Scott A. Wade,[2] Betty P. Kouskousis,[1,3] Daniel J. Kitcher,[1] Greg W. Baxter,[1] and Stephen F. Collins[1,*]

[1]*Optical Technology Research Laboratory, School of Engineering and Science, Victoria University, P.O. Box 14428, Melbourne, VIC 8001, Australia*
[2]*CAOUS, Swinburne University of Technology, Hawthorn, VIC 3122, Australia*
[3]*Now at CMP, Swinburne University of Technology, Hawthorn, VIC 3122, Australia*
**Corresponding author: stephen.collins@vu.edu.au*

Received December 9, 2011; accepted March 31, 2012;
posted April 16, 2012 (Doc. ID 159740); published June 6, 2012

The growth of reflectance peaks from optical fiber Bragg gratings has been studied to determine the relative importance of grating features when writing with the phase-mask technique. Measurements of spectra for two different fiber types using two distinct phase masks allowed the contribution from grating features of half the phase-mask periodicity and of the phase-mask periodicity at the Bragg wavelength to be determined. The dominance of the latter periodicity was ascribed to either the small fiber core diameter that limited the extent of the Talbot diffraction pattern, or the enhanced ±2 diffraction orders of a custom-made phase mask used. © 2012 Optical Society of America

OCIS codes: 060.3735, 060.3738, 070.6760, 050.2770.

1. INTRODUCTION

Since their discovery more than 20 years ago, optical fiber Bragg gratings (FBGs) have been investigated extensively, and used in a wide range of research and industrial applications as critical components in communications and sensing [1]. In its most basic form, an FBG consists of a periodic modulation of the refractive index along the optical fiber core that reflects light at wavelengths determined by the Bragg condition [1,2]. This refractive index modulation is usually imprinted when a periodic pattern of ultraviolet radiation is present in the core of certain fiber types; the responsiveness of this depends upon the fiber composition [3]. Various methods have been used for the fabrication of FBGs, with the most common method involving the use of a phase mask, as this ensures stability and reproducibility of grating properties [2]. In this approach, a continuous wave (CW) or pulsed UV laser beam is directed through a phase mask, of periodicity Λ_{pm}, resulting in an interference pattern, which, in turn, induces the corresponding refractive index variation along the fiber core of periodicity $\Lambda_{pm}/2$ [2]. The resultant Bragg wavelength, λ_B, is the first harmonic resonance (i.e., $m = 1$) given by the well-known Bragg formula [2]

$$\lambda_B(m) = \frac{2}{m} n_{\text{eff}} \Lambda, \tag{1}$$

where $\lambda_B(m)$ is the reflected wavelength at the harmonics $m = 1, 2, 3, \ldots$, and Λ is the grating period along the fiber core. The effective index of the fundamental fiber mode, n_{eff}, can be approximated as the refractive index of the fiber core at $\lambda_B(m)$. Phase masks are designed to provide maximum contrast for the interference of the ±1 diffraction orders, through elimination of the zero and higher diffraction orders. However, these undesired orders are not totally suppressed in a real phase mask, and experiments and simulations have shown that the interference of the nonsuppressed zeroth and higher diffraction orders of the phase mask result in a complex refractive index structure that exhibits an additional periodicity of $\Lambda = \Lambda_{pm}$, which coexists with the expected periodicity of $\Lambda = \Lambda_{pm}/2$ in an FBG [4–7]. Indeed, when the zeroth diffraction order was only 1% of the total power, the interference pattern and the corresponding refractive index variations written into polymers were affected significantly [8]. Importantly, the same coexisting FBG periodicities ($\Lambda_{pm}/2$ and Λ_{pm}) in a phase-mask-written FBG have been observed in images of gratings obtained using differential interference contrast (DIC) microscopy [9] and other techniques [10]. Through the use of modeling, based on the measured strengths of the diffraction orders of the phase mask used, the formation of the complex refractive index structure observed in DIC images has been verified [11].

The presence of the periodicity of the phase mask (i.e., Λ_{pm}) along a fiber core results in the occurrence of features at twice the Bragg wavelength, $2\lambda_B$, in accordance with Eq. (1), as inferred [12] and reported in experiments [13,14]. Conversely, for writing with pure ±1 diffraction orders in a Talbot interferometer arrangement, this second periodicity does not occur, and there are no grating features observed at twice the Bragg wavelength [15]. Grating resonance features of odd harmonics of this second periodicity, i.e., $2\lambda_B/3$ and $2\lambda_B/5$, have also been observed [16,17]. Generally the spectra near $2\lambda_B$, $2\lambda_B/3$, and $2\lambda_B/5$ exhibit a double peak/dip structure, as it is believed that the interleaved grating planes constitute a type of π-phase-shifted grating [14,18,19]. Grating features at other wavelengths though, notably $\lambda_B/2$ as reported by various authors [12,16,17], potentially arise from both periodicities and do not exhibit a double peak/dip

structure. Through a series of experiments, Xie *et al.* studied the induced refractive index change at both $\lambda_B/2$ and λ_B in type I FBGs written interferometrically (i.e., using only the ± 1 diffraction orders) in several fibers, showing that it exhibited a saturated exponential dependence on the UV fluence [12]. Indeed the second-order reflectance (i.e., $\lambda_B/2$) grew much slower than the first order.

As the primary feature, i.e., the "Bragg wavelength," in phase-mask-produced FBGs arises via coexisting periodicities of $\Lambda = \Lambda_{\mathrm{pm}}/2$ and Λ_{pm}, it is of interest to determine the relative contribution of each of these components to the reflection spectrum. By monitoring the evolution of FBG reflections at both $2\lambda_B/3$ and λ_B simultaneously and by analyzing the data at $2\lambda_B/3$ (which arises from Λ_{pm} only) using the model of Xie *et al.* [12], the contribution of $\Lambda_{\mathrm{pm}}/2$ to the reflection at λ_B may be determined. Thus, in this paper, the recorded spectral growth of harmonic reflections of type I FBGs is analyzed in terms of the Xie *et al.* model for reflectance growth as a function of fluence using two different fiber types (in particular having different core diameters). The use of a "custom-made" phase mask, in addition to a "standard" phase mask, provided enhancement of the Λ_{pm} periodicity via its enhanced ± 2 diffraction order.

2. THEORY

The reflectance of an FBG at a wavelength λ_m is given by [1]

$$R_m(l,\lambda_m) = \tanh^2\left(\frac{\pi \Delta n_m l \eta(\lambda_m)}{\lambda_m}\right), \tag{2}$$

where Δn_m is the amplitude of the induced refractive index change at λ_m, l is the grating length, and $\eta(\lambda_m)$ is the overlap between the fundamental mode and the index modulation at λ_m. The contributions of higher-order components can be determined from a Fourier expansion of the induced refractive index profile. Assuming that the index change profile of an FBG has a constant period Λ and is only a function of the distance along the fiber, z, the contributions of higher-order components to the induced refractive index profile can be described by [12]

$$\Delta n(z) = \Delta n_0 + \Delta n_1 \cos\left(\frac{2\pi z}{\Lambda} + \varphi_1\right) + \Delta n_2 \cos\left(\frac{4\pi z}{\Lambda} + \varphi_2\right) + \Delta n_3 \cos\left(\frac{6\pi z}{\Lambda} + \varphi_3\right) \ldots, 0 \le z \le l,$$
$$\Delta n(z) = 0, z > l, \tag{3}$$

where Δn_0 is determined experimentally using Eq. (2) and (φ_1, φ_2, φ_3) and (Δn_1, Δn_2, Δn_3) represent the first three terms of the Fourier phase and amplitude spectra, respectively.

The growth of the induced refractive index change during the fabrication of gratings in germanium-doped silica fiber without hydrogen or deuterium-presensitization can be described by a power law of the form $\Delta n \propto t^{\alpha}$, where α increases with power density [20,21]. Fibers that are presensitized with hydrogen or deuterium, however, normally follow a saturating exponential time t dependence of the form $\Delta n \propto 1 - \exp(-t/\tau)$ [22], where τ is a fitting parameter. The mechanisms for grating growth in the two fiber types are almost certainly different [23], with saturated exponential growth most likely related to the absorption of one UV photon, while power law growth is most likely related to multiple photon absorption.

Xie *et al.* [12] showed that the growth of the first- and second-order reflectances from an FBG are described by the dependence of the photoinduced index change $\Delta n(z,N)$ upon the number N of laser pulses and upon the local fluence of the beam impinging on the fiber:

$$\Delta n(z,N) = \Delta n_0\left(1 - e^{-kN\left(1+\cos\left(\frac{2\pi z}{\Lambda}\right)\right)}\right), \tag{4}$$

where k is a fitting parameter that is proportional to the intensity of the writing beam. Assuming the Fourier phase components are zero, the Fourier coefficients in Eq. (3) can be written as a function of z and N:

$$\Delta n_m(z,N) = \frac{2}{\Lambda}\int_0^{\Lambda} \Delta n_0\left(1 - e^{-kN\left(1+\cos\left(\frac{2\pi z}{\Lambda}\right)\right)}\right) \times \cos\left(\frac{2m\pi z}{\Lambda}\right) \mathrm{d}z, \text{ for } (m = 1,2,3\ldots). \tag{5}$$

The solutions of Eq. (5) are obtained numerically and, when substituted into Eq. (2), describe the growth with increasing fluence of harmonic reflectances from the FBG.

As CW laser radiation was used, exposure is described in terms of cumulative fluence, F in units of kJ/cm^2, instead of N. The fitting parameter, k, has units of (cm^2/kJ), and is likely to be codependent on many factors involved in the fabrication process, including the photosensitivity of the fiber, which was enhanced by hydrogen loading, the exact position of the fiber behind the phase mask, and the quality of the interference pattern formed behind the phase mask, which is ultimately photo-imprinted in the fiber core.

Data for the growth of the peak reflectance at $2\lambda_B/3$ were analyzed using Eq. (2) and the Xie *et al.* model for $\Delta n_m(z,N)$ using the $m = 3$ solution of Eq. (5) for $\Lambda = \Lambda_{\mathrm{pm}}$. To investigate the origins of reflections at λ_B, the model was applied to the measured growth of the peak reflectance at λ_B for both possible cases, i.e., for $m = 1$ of a grating with period $\Lambda = \Lambda_{\mathrm{pm}}/2$ and for $m = 2$ of a grating with period $\Lambda = \Lambda_{\mathrm{pm}}$. Since growth at $2\lambda_B/3$ can only be described by the $m = 3$ case for $\Lambda = \Lambda_{\mathrm{pm}}$, these data were fitted by varying the parameter k. Since spectral features at λ_B can result from the $m = 1$ reflection from a $\Lambda_{\mathrm{pm}}/2$ grating or from the $m = 2$ reflection from a $\Lambda = \Lambda_{\mathrm{pm}}$ grating, the two cases were first analyzed separately to investigate the contribution of each component. However, as the growth at λ_B is due to a combination of reflectances from both grating periods, the combined contribution, the total induced refractive index change at λ_B was considered as

$$\Delta n_T = a\Delta n_1(\lambda_B) + b\Delta n_2(\lambda_B), \tag{6}$$

where a and b are the weighting factors of the Fourier amplitudes $\Delta n_1(\lambda_B)$ and $\Delta n_2(\lambda_B)$, respectively. The induced refractive index change at λ_B is assumed to be due only to these components such that the sum of a and b is equal to 1. The measured reflectance growth at λ_B was then analyzed using a modified form of Eq. (2):

$$R(l,\lambda_B) = \tanh^2\left(\frac{\pi\Delta n_T l \eta(\lambda_B)}{\lambda_B}\right). \quad (7)$$

3. EXPERIMENTAL DETAILS

FBGs were written using 244 nm CW UV light from a Coherent Innova FreD Ar ion laser with maximum power of 120 mW. Two different phase masks were used, as listed in Table 1, where the average relative diffraction-order efficiencies were measured by placing an optical detector at a fixed distance behind the phase mask in the absence of a fiber. Various UV-grade optics were used to condition and focus the writing beam onto the fiber, and the width of the focused beam on the fiber was also controlled (determining the grating length, l).

Two fiber types were used, namely the standard telecommunications fiber (core diameter ~7.4 μm), from Optix, and Corning HI 1060 having a smaller core diameter (3.6 μm) and a cutoff wavelength of 930 ± 40 nm. These were hydrogen-loaded to enhance their photosensitivity. Samples were prepared by mechanical stripping of ~3 cm of the acrylate coating, and the cleaned bare fiber section was positioned parallel to the phase mask within approximately 150 μm.

Standard phase masks generally provide contributions of about 40% from the ±1 orders and less than 5% from the ±2 orders. In order to investigate the effect of different relative intensities in the orders produced by the phase mask, a custom-made phase mask from Ibsen Photonics was used in addition to a standard phase mask. This had approximately equal contributions from each of the ±1 and ±2 orders, while keeping the zeroth order low. Details of both phase masks are provided in Table 1.

In order to further understand the relative growth dynamics of spectral features in the region of $2\lambda_B/3$ and λ_B, the experimental arrangement shown in Fig. 1 was used to enable simultaneous measurement in both spectral regions during FBG fabrication. Light of central wavelengths of 1550 and 1040 nm, provided by an Er^{3+} broadband source (MPB Technologies EBS-7210) and a 1050 nm superluminescent diode (QPhotonics QSDM-1050-2), respectively, was coupled into the grating fiber using a 50:50 coupler. The unused arm of the coupler was placed in index-matching fluid to prevent spurious back-reflections. The output arm of the coupler was fusion spliced to the grating fiber, which was placed in the phase-mask fabrication arrangement. The output end of the exposed fiber sample was fusion spliced to a 2×1 coupler to separate the two wavelength bands (i.e., around 1040 and 1550 nm), which were recorded during fabrication by optical spectrum analyzers, Ando AQ-6315 E and Ando AQ-6317 B, operating at resolutions of 0.05 and 0.01 nm, respectively. By the use of two phase masks and two fiber types. four separate data sets were obtained, and analyzed according to the theory outlined in Section 2.

4. SIMULATION OF PHASE-MASK DIFFRACTION PATTERNS

In order to predict the refractive index patterns expected to be imprinted in the fiber core, the expected interference patterns were modeled [11] using the measured diffraction efficiencies up to ±2 for the two phase masks listed in Table 1, and assuming a writing wavelength $\lambda_w = 244$ nm, in a medium with index $n_w = 1.511$ (the index of silica at λ_w). As the index of the fiber core is slightly higher than the index of silica, there will be small differences in the Talbot lengths observed in FBG images. The simulated interference patterns for the standard and custom-made phase masks are shown in Figs. 2(a) and 2(b), respectively, and, as expected, reveal complex, interleaving regions of constructive and destructive interference due to beating between the multiple diffraction orders.

The plots featured in Figs. 2(c) and 2(d) are linescans along the direction parallel to the phase mask (z) through a region containing a maximum in the images in Figs. 2(a) and 2(b), respectively. Fast Fourier transforms (FFTs) of these z-linescans reveal a number of spectral components, which are summarized in Table 1 along with the relative strengths of each component in the FFT power spectrum. The dominant period in the standard phase-mask image in Fig. 2(a) is clearly half of the phase-mask period ($\Lambda_{pm}/2 \approx 0.53$ μm), as confirmed by the 92.5% relative strength of this period from the FFT analysis. The most dominant periods in the intensity pattern produced behind the custom-made phase mask are $\Lambda_{pm}/3$ and Λ_{pm}. As can be seen in Fig. 2(d), the custom-made phase-mask image exhibits features with a period of approximately 0.36 μm (corresponding to $\Lambda_{pm}/3$) that are just 30% of the intensity of features of period Λ_{pm}; consequently, they are expected to be unimportant in the refractive index structure induced in a fiber core. The increased contributions of the zeroth and ±2 diffraction orders of the custom-made phase mask have evidently caused the phase-mask period Λ_{pm} to dominate the interference pattern produced behind the mask. This result is consistent with the work of Dyer *et al.* [5], which reported that even small contributions from either of the

Table 1. Details of the Standard and Custom-Made Phase Masks, Their Measured Diffraction Orders, and the Deduced Spectral Components of the Simulated Diffraction Patterns in Fig. 2

		Measured					Analysis of simulations shown in Fig. 2		
		Average diffraction-order efficiencies (%)					z-direction		x-direction
Phase mask (Manufacturer)	Λ_{pm} (μm)	zeroth	±1st	±2nd	±3rd	±4th	Period (±0.01 μm) (fraction of Λ_{pm})	Normalized fast Fourier transform (FFT) strength (%)	Period (±0.01 μm)
Standard (Lasiris)	1.0668	1.8	39	3.5	3.3	3.3	0.53 (~1/2)	92.5	4.57
							1.11 (~1)	4.5	
							0.36 (~1/3)	3	
Custom (Ibsen Photonics)	1.07	3.2	15	19.6	13.5	0.4	0.36 (~1/3)	41.9	4.49
							1.11 (~1)	36.9	
							0.25 (~1/4)	13.1	
							0.53 (~1/2)	8.1	

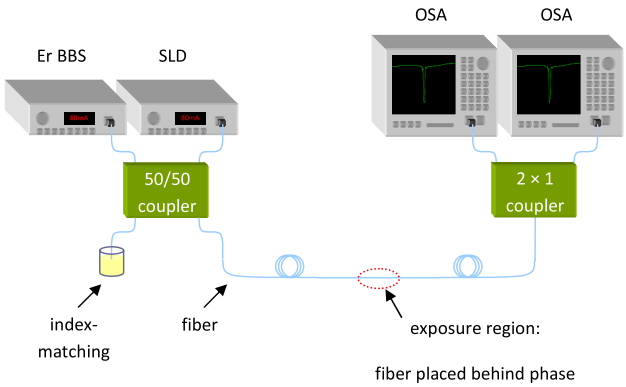

Fig. 1. (Color online) Schematic diagram of the experimental arrangement used for the simultaneous measurement of transmission spectra at λ_B and $2\lambda_B/3$ during fabrication using an erbium-doped fiber broadband source (Er BBS) and a superluminescent diode (SLD) operating near 1050 nm, respectively.

zeroth or ± 2 diffraction orders can cause Λ_{pm} features to dominate over $\Lambda_{pm}/2$ features. The Talbot lengths for Figs. 2(a) and 2(b), being the peak-to-peak distances in the x-linescans in Fig. 2(e), were about 4.6 μm, consistent with the expected values [7]. It is clear for the custom-made phase mask that the lower first order and higher zeroth and second orders affect the dominance of the periods present along the z-axis, resulting in the dominance of the Λ_{pm} period over the $\Lambda_{pm}/2$ period, and which in turn is expected to affect the strength of harmonic reflectances from these periods in the core of FBGs produced with this phase mask.

5. RESULTS

The spectral data obtained for the four FBGs are presented in the following subsections, and the sample parameters used in applying the Xie *et al.* model to these data are summarized in Table 2. The listed parameters include the grating length l and total UV fluence F_T. The Bragg wavelength, λ_B, is the maximum reflectance wavelength as inferred from transmission spectra measured after fabrication had finished, and the wavelength shift, $\Delta\lambda_B$, was inferred from $F = 0$ intercepts of linear fits applied to the evolution of λ_B with increasing fluence F, and a similar method was used for the features at $2\lambda_B/3$. The core and cladding indices were calculated using the known fiber parameters, thereby providing the normalized frequencies $V(\lambda_B)$ and $V(2\lambda_B/3)$. The effective indices $(n_{\text{eff}}(\lambda_B))$ and $(n_{\text{eff}}(2\lambda_B/3))$ and mode power fractions $\eta(\lambda_B)$ and $\eta(2\lambda_B/3)$ were calculated using Fimmwave software. The mean index changes $\Delta n_0(\lambda_B)$ and Δn_0 $(2\lambda_B/3)$ were inferred from the respective wavelength shifts [1].

A. Standard Phase Mask and Telecommunications Fiber (Grating A)

The transmission spectra at λ_B and $2\lambda_B/3$ of grating A, measured after fabrication, are shown in Figs. 3(a) and 3(b), respectively. The spectrum at λ_B shows a strong (saturated) dip with $R > 99.99\%$ centered at ~1546.3 nm (labeled as 1) that is accompanied by prominent cladding-mode losses at shorter wavelengths. In the region of $2\lambda_B/3$, where the fiber is multimoded, there are three smaller dips (labeled as 2, 3, and 4) with peak reflectances of about 33, 25, and 11.5% at

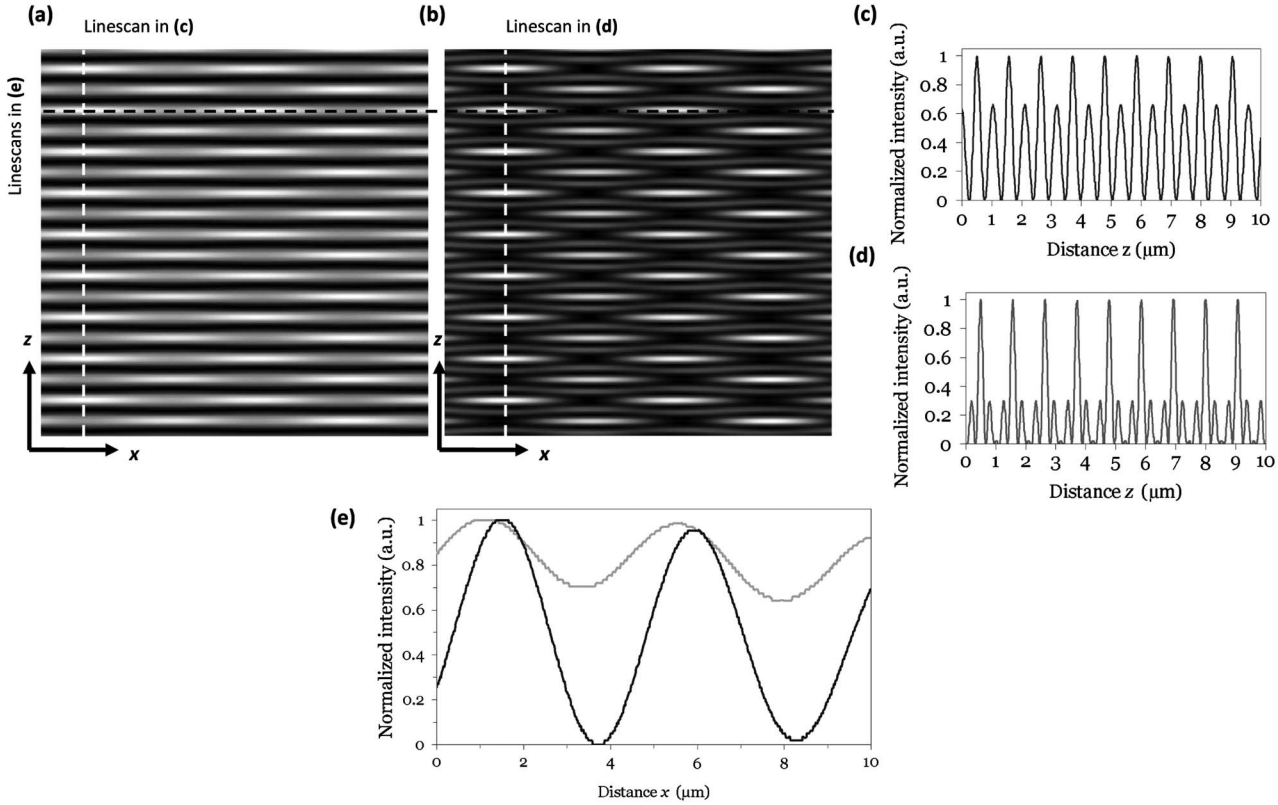

Fig. 2. Simulated intensity distributions behind UV irradiated phase masks in the region in which the fiber core lies during grating fabrication: (a) standard and (b) custom phase masks. The images represent a physical area of 10×10 μm. Linescans through the maximum intensity parallel to the phase mask in z for (c) standard and (d) custom phase masks. (e) Linescans through the maximum intensity perpendicular to the phase mask in x for standard and custom masks.

Table 2. Measured and Calculated Parameters of the Four Gratings Used in This Study

	Grating (fiber and phase mask)			
	A, Optix, Standard phase mask	B, Corning HI 1060, Standard phase mask	C, Optix, Custom phase mask	D, Corning HI 1060, Custom phase mask
l (±0.5 mm)	5.0	8.0	4.5	12.0
F_T (KJ/cm^2)	18 ± 3	5 ± 1	31 ± 6	10 ± 2
λ_B (±0.05 mm)	1546.30	1546.80	1551.10	1551.20
n_{cl} (λ_B) (±1 × 10^{-5})	1.44407	1.44406	1.44401	1.44401
n_{co} (λ_B) (±1 × 10^{-5})	1.45262	1.45850	1.45256	1.45845
V (λ_B) (±0.01)	2.37	1.50	2.36	1.50
$\Delta\lambda_B$ (±0.05 nm)	1.28	1.38	1.68	1.09
n_{eff} (λ_B) ±1×10^{-5}	1.44852	1.44732	1.44845	1.44724
η (λ_B) (±0.1)	0.8	0.5	0.8	0.5
Δn_0 (λ_B) (×10^{-3})	1.49 ± 0.04	2.6 ± 0.3	1.97 ± 0.05	2.1 ± 0.2
$2\lambda_B/3$ (±0.05 nm)	1033.10	1038.10	1038.04	1040.64
n_{cl} ($2\lambda_B/3$) (±1×10^{-5})	1.45001	1.44995	1.44995	1.44991
n_{co} ($2\lambda_B/3$) (±1×10^{-5})	1.45856	1.46444	1.45850	1.46441
V ($2\lambda_B/3$) (±0.01)	3.55	2.24	3.53	2.23
Δ ($2\lambda_B/3$) (±0.05 nm)	0.56	1.49	1.28	0.97
n_{eff} ($2\lambda_B/3$) (±1×10^{-5})	1.45622	1.45700	1.45615	1.45695
η ($2\lambda_B/3$) (±0.1)	0.9	0.7	0.9	0.7
Δn_3 (λ_3) (×10^{-3})	0.87 ± 0.01	3.0 ± 0.4	1.99 ± 0.03	1.9 ± 0.2

1033.1, 1034.1, and 1035.1 nm, respectively. The wavelength shifts during fabrication of the labeled spectral features were linear towards longer wavelengths, as expected for type I FBGs.

The reflectance growth of the spectral features labeled 1 (at λ_B) and 2 (at $2\lambda_B/3$) in Figs. 3(a) and 3(b), respectively, are plotted in Fig. 4. Clearly the growth of the reflectance peak at $2\lambda_B/3$ is much slower than the growth at λ_B, as expected for higher harmonic reflections. The data at $2\lambda_B/3$ were fitted with the Xie *et al.* model for $m = 3$ and $\Lambda = \Lambda_{pm}$, as shown by the dotted lines in Fig. 4, giving $k = 0.114$ cm^2/kJ (with $r^2 = 0.98$). On the other hand, attempted fits for the growth of the reflectance peak at λ_B, firstly for $m = 1$ with $\Lambda = \Lambda_{pm}/2$, and secondly for $m = 2$ with $\Lambda = \Lambda_{pm}$, resulted in a poor description of the data, as shown in Fig. 4(a) by the solid and short dashed lines, respectively. However, when the λ_B data were analyzed as a combination of these components [Fig. 4(a)], the weighting factors $a = 39.50 \pm 0.5\%$ and $b = 60.50 \pm 0.5\%$ provided the fit shown in Fig. 4(b) by the long dashed line having $r^2 = 0.996$. Although the data for λ_B appears to be more closely described by the modeled growth of the $m = 1$ component of a grating with a period $\Lambda_{pm}/2$, the greater percentage contribution to the observed reflectance growth provided by the $m = 2$ component of a grating of periodicity Λ_{pm} arises as reflectance is proportional to $\tanh^2$ of the induced refractive index change, and so a higher contribution to the induced refractive index change has resulted in a smaller effect on the reflectance growth. Clearly, the formation of the usual Bragg grating reflection peak is influenced significantly by the second harmonic reflection from grating features with a period equal to the phase mask.

B. Standard Phase Mask and Small-Core Fiber (Grating B)

The transmission spectra of grating B after fabrication measured at λ_B and $2\lambda_B/3$ are shown in Figs. 3(c) and 3(d), respectively. At λ_B, there is a strong dip with $R > 99.99\%$ centered at ~1546.8 nm (labeled as 5) that is accompanied by strong cladding-mode losses, and which has almost double the width of the dip at λ_B of grating A, despite being exposed to a much lower total UV fluence. As seen in the corresponding reflectance versus fluence plots in Figs. 4 and 5, the reflectance at λ_B of grating A began to saturate after an exposure fluence of approximately 7 kJ/cm^2, whereas the reflectance of grating B began to saturate after only 2 kJ/cm^2. This may be due to a number of factors, including Corning HI 1060 fiber having a higher Ge content in the core than the Optix fiber, leading to higher photosensitivity, and the larger grating length of grating B ($l \sim 8$ mm) producing stronger reflections than from the shorter grating A ($l \sim 5$ mm). The cladding-mode losses on the short wavelength side of λ_B of the less-saturated grating A are stronger than those of grating B and are possibly due to a higher total UV fluence, a longer grating length, or a slight tilt in the phase mask during fabrication [24]. The spectrum of grating B in the region of $2\lambda_B/3$ shows two prominent features (labeled as 6 and 7) with peak reflectances of about 99.7 and 98% at approximately 1038.1 and 1034.6 nm, respectively. The wavelength shifts during fabrication of the labeled spectral features were also linear towards longer wavelengths, as expected for type I FBGs. The features labeled 6 and 7 in Fig. 3(d) both exhibit a double transmission dip structure, as discussed in Section 1; feature 7 is likely to be due to cladding modes, and feature 6 is saturated due to prolonged exposure.

The spectral features at $2\lambda_B/3$ are much stronger in grating B when the fiber is single mode than for grating A, in which the fiber is multimoded, which may be due to the larger grating length l. Importantly, under single mode conditions, the fundamental mode is much more tightly confined to the core, and so a greater fraction of the propagating optical power interacts with the refractive index structure in the core, resulting in stronger reflectances than in multimode fiber. This is supported by Fig. 5, which shows that under single mode conditions, the peak reflectances of the spectral features in both regions demonstrate similar growth characteristics. This is in

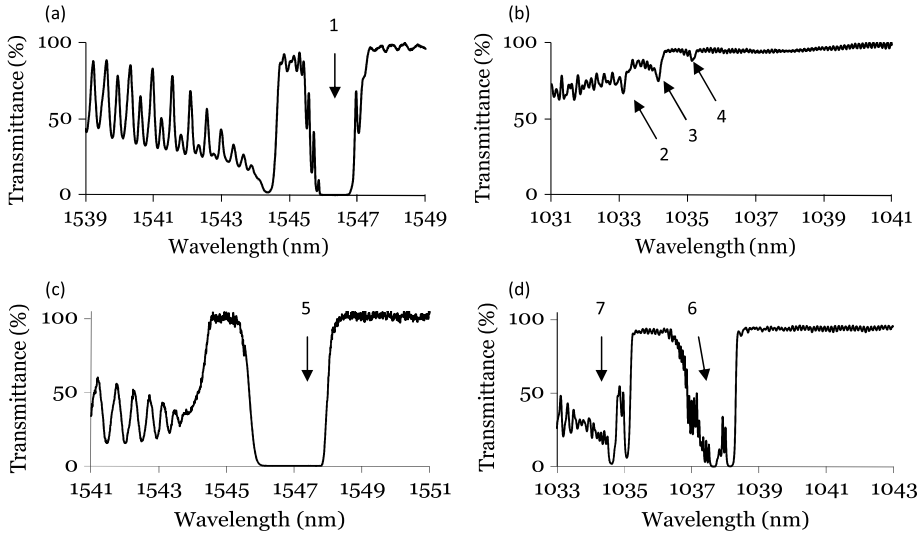

Fig. 3. Spectral properties FBGs fabricated using a standard phase mask in the two fiber types. Transmission spectra measured after fabrication of grating A: (a) at λ_B and (b) at $2\lambda_B/3$; and of grating B: (c) at λ_B and (d) at $2\lambda_B/3$.

contrast to Fig. 4 (grating A), where features at $2\lambda_B/3$, propagating under multimode conditions, exhibit much slower peak reflectance growth than for the single mode features at λ_B. The measured reflectance growth of the spectral features labeled 5 (at λ_B) and 6 (at $2\lambda_B/3$) in Figs. 3(c) and 3(d), respectively, are plotted in Fig. 5.

The growth of the reflectance peak at $2\lambda_B/3$ was fitted with the Xie *et al.* model for $m = 3$ and $\Lambda = \Lambda_{\mathrm{pm}}$, as shown by the dotted line in Fig. 5; the best fit provided $k = 0.94\ \mathrm{cm}^2/\mathrm{kJ}$ (with $r^2 = 0.99$). The resulting fits for the growth of the reflectance peak at λ_B firstly for $m = 1$ with $\Lambda = \Lambda_{\mathrm{pm}}/2$ and secondly for $m = 2$ with $\Lambda = \Lambda_{\mathrm{pm}}$ are shown in Fig. 5(a) by the solid and short dashed lines, respectively. The data are described well when the reflection at λ_B is considered as the second harmonic ($m = 2$) of a grating with a Λ_{pm} period with $r^2 = 0.99$. Indeed, a fit with a combination of both components as given by Eq. (7) provided only a slight

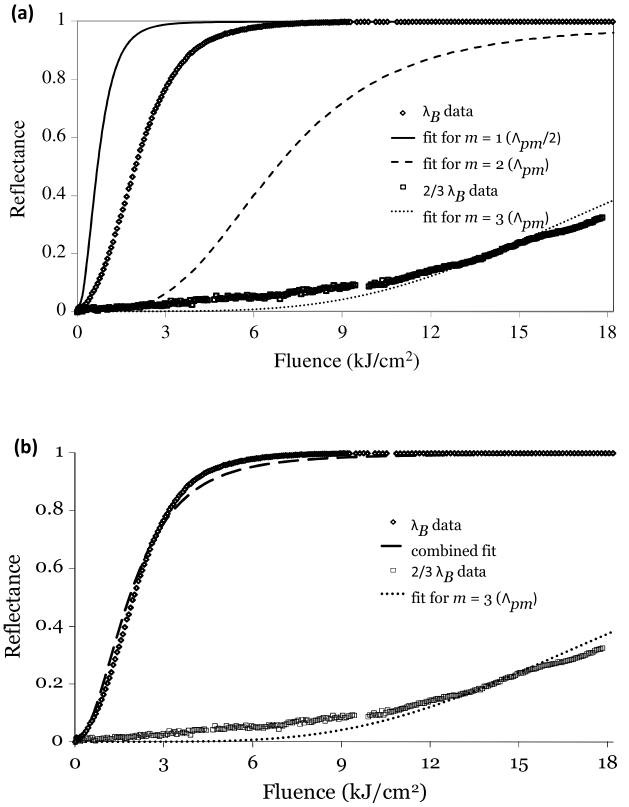

Fig. 4. Measured and modeled reflectance growth of spectral features at λ_B and $2\lambda_B/3$ of grating A: (a) with fits for λ_B as $m = 1$ of a $\Lambda_{\mathrm{pm}}/2$ grating, for λ_B as $m = 2$ of a Λ_{pm} grating, and for $2\lambda_B/3$ as $m = 3$ of a Λ_{pm} grating; (b) with fits for λ_B as a combination of both harmonic components and for $2\lambda_B/3$ as $m = 3$ of a Λ_{pm} grating.

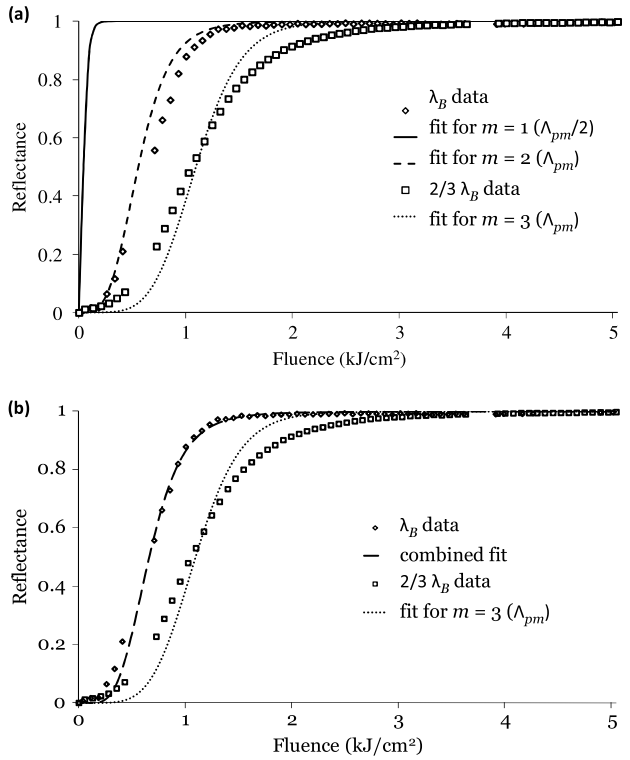

Fig. 5. Measured and modeled reflectance growth of spectral features at λ_B and $2\lambda_B/3$ of grating B: (a) with fits for λ_B as $m = 1$ of a $\Lambda_{\mathrm{pm}}/2$ grating, for λ_B as $m = 2$ of a Λ_{pm} grating and for $2\lambda_B/3$ as $m = 3$ of a Λ_{pm} grating; (b) with fits for λ_B as a combination of both harmonic components and for $2\lambda_B/3$ as $m = 3$ of a Λ_{pm} grating.

improvement to the fit as shown in Fig. 5(b) by the long dashed line, in which the factors were $a = 3 \pm 0.5\%$ and $b = 97 \pm 0.5\%$. The data in Fig. 5 are described quite well by the Xie *et al.* model for the second and third harmonics of a structure dominated by the Λ_{pm} period. Discrepancies between the data and the fits are seen mainly in the slopes of the reflectance growth prior to saturation, which is reached at approximately $F = 2$ kJ/cm^2 for λ_B and $F = 3$ kJ/cm^2 for $2\lambda_B/3$. The discrepancies in the slopes are most likely due to uncertainties associated with estimating the induced refractive index changes and other fitting parameters. These results indicate that when features in both spectral regions are under single mode conditions (grating B), the peak reflectances demonstrate similar growth characteristics, while the reflectance growth of features at $2\lambda_B/3$ under multimode conditions, in the case of grating A, is much slower than the growth of single mode features at λ_B.

C. Custom Phase Mask and Telecommunications Fiber (Grating C)

Grating C was fabricated using the custom-made phase mask, in the hydrogen-loaded telecommunications fiber with a total fluence of approximately 31 kJ/cm^2. As for grating A, the fiber was single mode in the region of λ_B but multimode in the region of $2\lambda_B/3$. To reach similar levels of saturation, this FBG required exposure to approximately double the fluences of the standard phase-mask FBGs, since the custom-made phase mask provided approximately half the first-order contribution of the standard phase mask.

The transmission spectra measured after fabrication at λ_B and $2\lambda_B/3$ are shown in Figs. 6(a) and 6(b), respectively. The spectra at λ_B shows a strong dip with $R = 95.8\%$ centered at ~1551.1 nm (labeled as 1), which has almost no cladding-mode losses on the short wavelength side, and which is quite narrow, indicating minimal saturation. The spectra in the region of $2\lambda_B/3$ shows two sets of double-dip structures (labeled as 2 and 3) with peak reflectances of approximately 38 and 54% at approximately 1038 and 1037 nm, respectively; the origins of such double-dip structures were discussed in Section 1. The peak wavelength shifts during fabrication of the labeled spectral features were linear towards longer wavelengths, as expected for type I growth, even though this grating exhibited two phases of reflectance growth, most likely caused by an interruption (e.g., a drop in the power of the UV laser or a disruption to the beam or fiber position) to the UV exposure conditions during fabrication.

Comparison of spectra from gratings A and C, written with the standard and custom-made phase masks, respectively, show that the custom-made phase mask produced stronger reflectances in the multimode region of $2\lambda_B/3$. The peak reflectance was 33% in the region of $2\lambda_B/3$ for the standard mask [Fig. 3(b)], whereas the peak reflectance was 54% for the custom-made mask [Fig. 6(b)]. Since spectral features in the region of $2\lambda_B/3$ correspond to the third harmonic reflection from a grating with a period of Λ_{pm}, their observed peak reflectance increase can therefore be attributed to dominance of the period Λ_{pm} arising from the higher contributions from the zeroth and ± 2 orders from the custom-made phase mask.

The measured reflectance growth of the spectral features labeled 1 (at λ_B) and 2 (at $2\lambda_B/3$) in Figs. 6(a) and 6(b), respectively, are plotted in Fig. 7. The growth of both reflectance peaks exhibited two phases of growth, one of which slowed after $F \approx 9$ kJ/cm^2 and began to grow again at around 12 kJ/cm^2. Although reminiscent of type IIA growth, this is highly unlikely in this hydrogen-loaded standard telecommunications fiber, since type IIA growth is typically observed in high germanium and codoped fibers only [3]. Normal type I growth was evident from the observed linear shifts in peak reflectance wavelengths, confirming that this abnormal growth was caused by an interruption. The Xie *et al.* model was applied to the second growth phase of the reflectance peaks; i.e., data for fluences >12 kJ/cm^2 were treated as normal type I growth.

The fit to the second growth phase of the reflectance peak at $2\lambda_B/3$, from $F \approx 12$ kJ/cm^2 onwards, for $m = 3$ and $\Lambda = \Lambda_{pm}$, is shown by the dotted lines in Fig. 7; the best fit produced $k = 0.044$ cm^2/kJ (with $r^2 = 0.98$). The resulting fits for the second growth phase of the reflectance peak at λ_B, firstly for $m = 1$ with $\Lambda = \Lambda_{pm}/2$ and secondly for $m = 2$ with $\Lambda = \Lambda_{pm}$, are shown in Fig. 7(a) by the solid and short dashed lines, respectively.

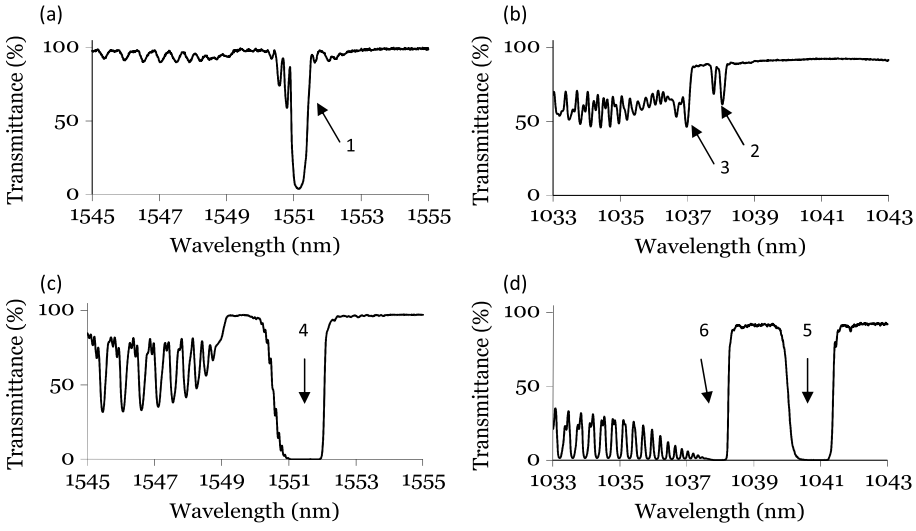

Fig. 6. Spectral properties of FBGs fabricated using a custom-made phase mask in the two fiber types. Transmission spectra measured after fabrication of grating C: (a) at λ_B and (b) at $2\lambda_B/3$; and grating D: (c) at λ_B and (d) at $2\lambda_B/3$.

As can be seen in Fig. 7(a), describing the reflection at λ_B as just the second harmonic ($m = 2$) of a grating with a Λ_{pm} periodicity gives a reasonable approximation of the data. When the data were fitted as a combination of both components given by Eq. (7), the resulting weighting factors of $a = 5 \pm 0.5\%$ and $b = 95 \pm 0.5\%$ provided the long dashed line shown in Fig. 7(b) (with $r^2 = 0.89$). Thus the observed reflectance growth at λ_B for grating C is due predominantly to second harmonic reflections from the Λ_{pm} period features, which is consistent with the characteristics of the intensity distributions of the custom-made phase mask. The growth of the reflectance peak at $2\lambda_B/3$ was slower than the growth of the reflectance peak at λ_B, which resembles the delay observed for the multimode grating A between the growths at $2\lambda_B/3$ and λ_B. However, the growth at both wavelengths was relatively faster for grating C using the custom-made phase mask and larger core fiber, which is attributed to the dominance of the Λ_{pm} period in this case.

D. Custom Phase Mask and Small-Core Fiber (Grating D)

Use of the custom-made phase mask and hydrogen-loaded Corning HI 1060 fiber with a total fluence of approximately 10 kJ/cm^2 resulted in grating D, having the transmission spectra in the regions about λ_B and $2\lambda_B/3$, shown in Figs. 6(c) and 6(d), respectively. The spectra at λ_B shows a strong dip with $R > 99.99\%$ centered at ~1551.2 nm (labeled as 4), which is accompanied by much stronger cladding-mode losses than grating C near λ_B. The main transmission dip at λ_B is much more saturated than that of grating C with more than double the spectral width. The spectra at $2\lambda_B/3$ shows the main dip with $R = 99.99\%$ centered at ~1040.6 nm (labeled as 5), which is accompanied by very strong cladding-mode losses on the short wavelength side (labeled as 6). The main transmission dip at $2\lambda_B/3$ is almost as broad as the dip at λ_B. The wavelength shifts during fabrication of the labeled spectral features were linear towards longer wavelengths, as expected for type I FBGs.

The reflectance growth of the spectral features labeled 4 (at λ_B) and 5 (at $2\lambda_B/3$) in Figs. 6(c) and 6(d), respectively, are plotted in Fig. 8. The stronger cladding-mode losses at both $2\lambda_B/3$ and λ_B are possibly due to the longer grating length (~12 mm for grating D and ~5 mm for grating C) or a slight tilt in the phase mask during fabrication. The transmission dip at λ_B is much broader than the dip at λ_B of grating C, despite being exposed to a much lower UV fluence. As previously discussed for gratings A and B, this is likely to be due to greater reflectance saturation resulting from higher fiber photosensitivity, longer grating length, and higher modal confinement to the core in grating D. The spectral features at $2\lambda_B/3$ are much stronger in the single-moded grating D than for grating C, which was multimode. As discussed above, this may be due to grating D being longer, but also since, under single mode conditions, the fundamental mode is much more tightly confined to the core, resulting in greater interaction with the grating and stronger reflectances.

Comparison of gratings B and D in the region of $2\lambda_B/3$ (i.e., where the fiber is single-moded) written with the standard and custom-made phase masks, respectively, shows that the custom-made phase mask produced stronger reflections. In fact, the spectral features at $2\lambda_B/3$ for grating D are approximately 10 dB stronger than the features for grating B, and features are much more saturated for grating D, indicating that larger refractive index changes have been induced in the core due to the use of the custom-made phase mask. The repeat (Talbot) length [7], Z_T, of the intensity patterns formed perpendicular to the phase masks is ~4.6 μm, but the diameter of the fiber core is only ~3.6 μm. It is conceivable that the core of the single mode fiber is not large enough to allow the $\Lambda_{pm}/2$ period to dominate the structure imprinted in the fiber core, leading to similar reflectances in the standard and custom-made mask gratings.

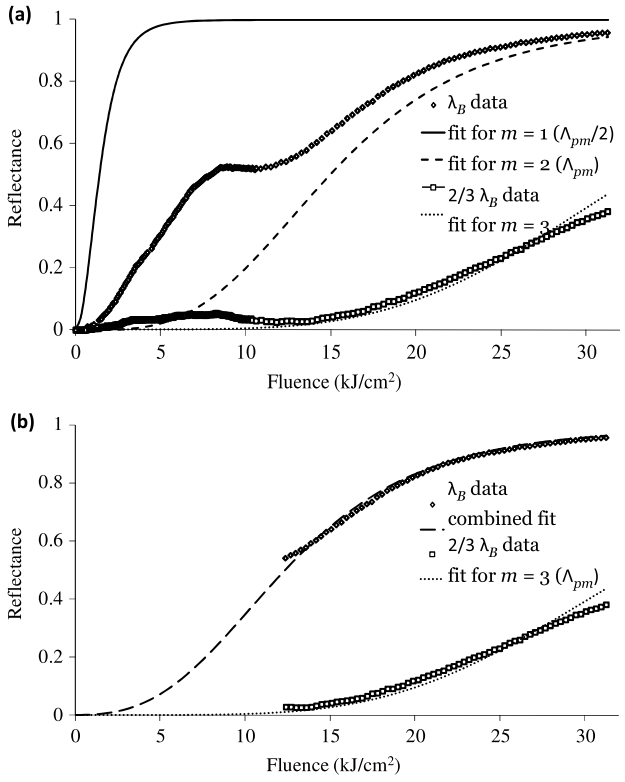

Fig. 7. Measured and modeled reflectance growth of spectral features at λ_B and $2\lambda_B/3$ of grating C: (a) with fits for λ_B as $m = 1$ of a $\Lambda_{pm}/2$ grating, for λ_B as $m = 2$ of a Λ_{pm} grating and for $2\lambda_B/3$ as $m = 3$ of a Λ_{pm} grating; (b) with fits for λ_B as a combination of both harmonic components and for $2\lambda_B/3$ as $m = 3$ of a Λ_{pm} grating (low fluence data omitted due to interruption during inscription).

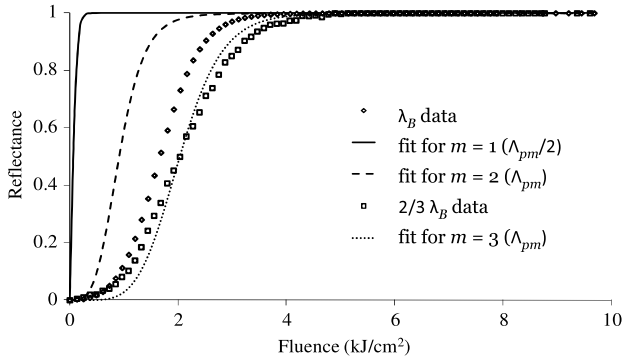

Fig. 8. Measured and modeled reflectance growth of spectral features at λ_B and $2\lambda_B/3$ of grating D—with fits for λ_B as $m = 1$ of a $\Lambda_{pm}/2$ grating, for λ_B as $m = 2$ of a Λ_{pm} grating and for $2\lambda_B/3$ as $m = 3$ of a Λ_{pm} grating.

The growth of the reflectance peak at $2\lambda_B/3$ was fitted with the Xie *et al.* model for $m = 3$ and $\Lambda = \Lambda_{pm}$, as shown by the dotted line in Fig. 8. The best fit yielded $k = 0.515$ cm^2/kJ (with $r^2 = 0.99$). The resulting fits for the growth of the reflectance peak at λ_B, firstly for $m = 1$ with $\Lambda = \Lambda_{pm}/2$ and secondly for $m = 2$ with $\Lambda = \Lambda_{pm}$, are shown by the solid and short dashed lines, respectively. The best fit to the data ($r^2 = 0.80$) had the reflection at λ_B being described as the second harmonic ($m = 2$) of a grating with a Λ_{pm} period. Considering the reflectance growth at λ_B as being due to a combination of both harmonic components, given by Eq. (7), provided no improvement to the fit to the data over the case for $m = 2$ with $\Lambda = \Lambda_{pm}$ alone.

These results suggest that Λ_{pm} is the dominant period in the refractive index structure that exists in the core of grating D, consistent with the fact that the reflectances at $2\lambda_B/3$ of both the standard and custom-made mask grating were much stronger than for the multimode, larger core gratings, and also consistent with the properties of the custom-made phase mask.

The observed growths in the two spectral regions, however, are more similar than predicted by the Xie *et al.* model. The growth of the reflectance peak at $2\lambda_B/3$ was observed to be almost coincident with the growth of the reflectance peak at λ_B, which is attributed firstly to the single-moded nature of the fiber at both wavelengths and secondly to the dominance of Λ_{pm} features in the pattern provided by the custom-made phase mask. The measured growth of λ_B of grating D is actually slower than the predicted growth shown in Fig. 8. As mentioned previously, the discrepancies in the slopes are most likely due to uncertainties associated with estimating the induced refractive index changes and other fitting parameters. This result for the custom-made phase mask indicates that when features in both spectral regions are under single mode conditions, the peak reflectances demonstrate similar growth characteristics. In contrast, when features at $2\lambda_B/3$ are propagating under multimode conditions, the peak reflectance growth is much slower than for the single mode features at λ_B.

6. DISCUSSION

The reflectance growth modelling is summarized in Table 3, which shows the contributions to the reflectance growth at λ_B from the $m = 2$ (for Λ_{pm}) and $m = 1$ (for $\Lambda_{pm}/2$) components. It can be seen that the Λ_{pm} periodicity was dominant for all four gratings, which was to be expected for those fabricated using the custom-made phase mask (gratings B and D) given the simulated intensity distribution in Fig. 2(e). However, for gratings A and C, the use of a standard phase mask was expected to favor the $\Lambda_{pm}/2$ periodicity and thus, as seen in Figs. 4 and 7, this periodicity dominated the early stages of grating growt,h in contrast to Figs. 5 and 8 (FBGs B and D, respectively).

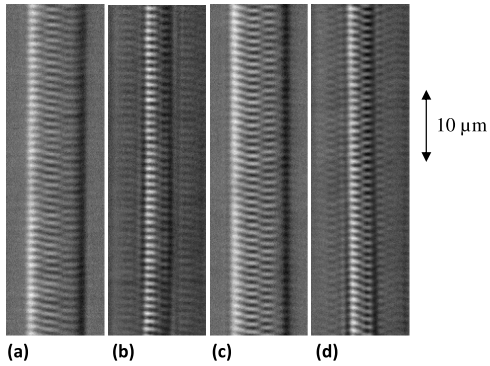

Fig. 9. DIC images showing the imprinted Talbot diffraction patterns of the type I FBGs investigated written with (a) phase mask in telecommunications fiber (grating A), (b) standard phase mask in smaller core fiber (grating B), (c) custom-made phase mask in telecommunications fiber (grating C), and (d) custom-made phase mask in smaller core fiber (grating D). The images are approximately 47×14 μm.

To provide further information about the imprinted grating structures relative to the fiber core DIC images of the four gratings, obtained in the plane perpendicular to the writing beam using methodology described elsewhere [9,11] and having a resolution of about 200 nm, are shown in Fig. 9. The measured Talbot lengths, the distance over which the diffraction pattern repeats itself, in the images were consistent with the expected value [7] of 4.6 μm and are of a similar magnitude to the fiber core diameters. For standard telecommunications fiber (i.e., gratings A and C) in Figs. 9(a) and 9(c), respectively, it can be seen that more than one full Talbot pattern (~1.6 times) is imprinted in the core. However, when about only 80% of one full Talbot pattern was imprinted in the core of the smaller core fiber (gratings B and D in Figs. 9(b) and 9(d), respectively), there was only one region along the fiber core where adjoining out-of-phase fringes were interleaved. Since this is responsible for the $\Lambda_{pm}/2$ structure, the lack of strength for the growth at λ_B in FBGs B and D, as shown in Figs. 5 and 8, respectively, is unsurprising.

The enhanced growth at $2\lambda_B/3$ (gratings B and D), compared with the corresponding gratings in fiber that is multimoded at that wavelength (gratings A and C), is because the fundamental mode is much more tightly confined to the core, thereby allowing a greater fraction of the propagating mode to interact with the refractive index structure. Conversely, for grating A, the reflectance growth at λ_B using the standard phase mask had an appreciable contribution from the $\Lambda_{pm}/2$ period, as the larger core size allowed this periodicity

Table 3. Summary of the Grating Properties and the Modeled Contributions of Spectral Components to the Reflectance Growth for Spectral Features at λ_B

Grating	Fiber	Core diameter (μm)	Phase-mask pitch	Contribution from $m = 1$ of $\Lambda_{pm}/2$ *a* (%)	Contribution from $m = 2$ of Λ_{pm} *b* (%)
A	Optix	7.4	Standard: 1.0668 μm	39.5	60.5
B	1060	3.6		3	97
C	Optix	7.4	Custom: 1.07 μm	5	95
D	1060	3.6		0	100

to be imprinted several times along the fiber core, as evident in Fig. 9(a).

7. CONCLUSION

The growth of the reflectance of spectral features of optical FBGs at λ_B and $2\lambda_B/3$ as a function of exposure fluence, fabricated in standard and smaller core fibers with standard and custom-made phase masks, have been analyzed in terms of the model proposed by Xie *et al.* [12] for type I FBGs, in conjunction with modelling of the expected diffraction fields and DIC images of the fabricated gratings. As spectral features at $2\lambda_B/3$ occur only as a third harmonic reflection from a grating with a period equal to the phase mask, Λ_{pm}, the growth of the peak reflectance at $2\lambda_B/3$ with increasing fluence was analyzed so that the contributions of the coexisting grating periodicities, Λ_{pm} and $\Lambda_{\mathrm{pm}}/2$, to spectral features at λ_B could be determined. The dominance of the Λ_{pm} periodicity, rather than $\Lambda_{\mathrm{pm}}/2$, in the development of spectral features at λ_B for three of the four gratings investigated was explicable either through the small fiber core diameter or the enhanced ± 2 diffraction orders of the custom-made phase mask.

The results presented here show that the complex refractive index pattern within phase-mask-produced optical FBGs contribute very significantly to observed spectral properties. Imaging plays an important role in understanding grating performance, and the ability to relate images and spectral features is the subject of ongoing research. Indeed, to fabricate FBGs tailored to a given application requires a detailed understanding of the role of fiber geometry and phase-mask properties, in addition to fiber material type and preparation.

ACKNOWLEDGMENTS

The authors acknowledge the financial support of the Australian Research Council. C. M. Rollinson and B. P. Kouskousis thank Victoria University for postgraduate scholarships. The authors acknowledge the School of Physics at The University of Melbourne for access to Fimmwave software.

REFERENCES

1. A. Othonos and K. Kalli, *Fiber Bragg Gratings* (Artech House, 1999).
2. K. O. Hill and G. Meltz, "Fiber Bragg grating technology fundamentals and overview," J. Lightwave Technol. **15**, 1263–1276 (1997).
3. J. Canning, "Fibre gratings and devices for sensors and lasers," Laser Photon. Rev. **2**, 275–289 (2008).
4. P. E. Dyer, R. J. Farley, R. Giedl, C. Ragdale, and D. Reid, "Study and analysis of submicron-period grating formation on polymers ablated using a KrF laser irradiated phase mask," Appl. Phys. Lett. **64**, 3389–3391 (1994).
5. P. E. Dyer, R. J. Farley, and R. Giedl, "Analysis of grating formation with excimer laser irradiated phase masks," Opt. Commun. **115**, 327–334 (1995).
6. P. E. Dyer, R. J. Farley, and R. Giedl, "Analysis and application of a 0/1 order Talbot interferometer for 193 nm laser grating formation," Opt. Commun. **129**, 98–108 (1996).
7. J. D. Mills, C. W. J. Hillman, B. H. Blott, and W. S. Brocklesby, "Imaging of free-space interference patterns used to manufacture fiber Bragg gratings," Appl. Opt. **39**, 6128–6135 (2000).
8. Z. Xiong, G. D. Peng, B. Wu, and P. L. Chu, "Effects of the zeroth-order diffraction of a phase mask on Bragg gratings," J. Lightwave Technol. **17**, 2361–2365 (1999).
9. N. M. Dragomir, C. Rollinson, S. A. Wade, A. J. Stevenson, S. F. Collins, G. W. Baxter, P. M. Farrell, and A. Roberts, "Nondestructive imaging of a type I optical fiber Bragg grating," Opt. Lett. **28**, 789–791 (2003).
10. C. W. Smelser, S. J. Mihailov, D. Grobnic, P. Lu, R. B. Walker, H. Ding, and X. Dai, "Multiple-beam interference patterns in optical fiber generated with ultrafast pulses and a phase mask," Opt. Lett. **29**, 1458–1460 (2004).
11. B. P. Kouskousis, C. M. Rollinson, D. J. Kitcher, S. F. Collins, G. W. Baxter, S. A. Wade, N. M. Dragomir, and A. Roberts, "Quantitative investigation of the refractive-index modulation within the core of a fiber Bragg grating," Opt. Express **14**, 10332–10338 (2006).
12. W. X. Xie, M. Douay, P. Bernage, P. Niay, J. F. Bayon, and T. Georges, "Second order diffraction efficiency of Bragg gratings written within germanosilicate fibres," Opt. Commun. **101**, 85–91 (1993).
13. P. E. Dyer, R. J. Farley, R. Giedl, K. C. Byron, and D. Reid, "High reflectivity fibre gratings produced by incubated damage using a 193 nm ArF laser," Electron. Lett. **30**, 860–862 (1994).
14. S. P. Yam, Z. Brodzeli, B. P. Kouskousis, C. M. Rollinson, S. A. Wade, G. W. Baxter, and S. F. Collins, "Fabrication of a π-phase-shifted fiber Bragg grating at twice the Bragg wavelength with the standard phase mask technique," Opt. Lett. **34**, 2021–2023 (2009).
15. S. P. Yam, Z. Brodzeli, S. A. Wade, G. W. Baxter, and S. F. Collins, "Occurrence of features of fiber Bragg grating spectra having a wavelength corresponding to the phase mask periodicity," J. Electron. Sci. Tech. China **6**, 458–461 (2008).
16. B. Malo, D. C. Johnson, F. Bilodeau, J. Albert, and K. O. Hill, "Single-excimer-pulse writing of fiber gratings by use of a zero-order nulled phase mask: grating spectral response and visualization of index perturbations," Opt. Lett. **18**, 1277–1279 (1993).
17. C. M. Rollinson, S. A. Wade, N. M. Dragomir, G. W. Baxter, S. F. Collins, and A. Roberts, "Reflections near 1030 nm from 1540 nm fibre Bragg gratings: evidence of a complex refractive index structure," Opt. Commun. **256**, 310–318 (2005).
18. C. M. Rollinson, S. A. Wade, N. M. Dragomir, A. Roberts, G. W. Baxter, and S. F. Collins, "Three parameter sensing with a single Bragg grating in non-birefringent fiber," in *Proceedings of Topical Meeting on Bragg Gratings, Poling, and Photosensitivity (BGPP)* (Engineers Australia, 2005), pp. 92–94.
19. S. P. Yam, G. W. Baxter, S. A. Wade, and S. F. Collins, "Modelling of an alternative pi-phase-shifted fibre Bragg grating operating at twice the Bragg wavelength," in *35th Australian Conference on Optical Fibre Technology (ACOFT)* (Australian Institute of Physics, Australian Optical Society, and Engineers Australia, 2010), p. 659.
20. D. Z. Anderson, V. Mizrahi, T. Erdogan, and A. E. White, "Production of in-fibre gratings using a diffractive optical element," Electron. Lett. **29**, 566–568 (1993).
21. H. Patrick and S. L. Gilbert, "Growth of Bragg gratings produced by continuous-wave ultraviolet light in optical fiber," Opt. Lett. **18**, 1484–1486 (1993).
22. T. A. Strasser, T. Erdogan, A. E. White, V. Mizrahi, and P. J. Lemaire, "Ultraviolet laser fabrication of strong, nearly polarization-independent Bragg reflectors in," Appl. Phys. Lett. **65**, 3308 (1994).
23. B. Poumellec and F. Kherbouche, "The photorefractive Bragg gratings in the fibers for telecommunications," J. Phys. III **6**, 1595–1624 (1996).
24. T. Erdogan and J. E. Sipe, "Radiation-mode coupling loss in tilted fiber phase gratings," Opt. Lett. **20**, 1838–1840 (1995).